Highly polarized electrons from GaAs–GaAsP and InGaAs–AlGaAs strained-layer superlattice photocathodes

T. Nishitani, T. Nakanishi,[a] M. Yamamoto, S. Okumi, F. Furuta, M. Miyamoto, M. Kuwahara, N. Yamamoto, and K. Naniwa
Department of Physics, Graduate School of Science, Nagoya University, Nagoya 464-8602, Japan

O. Watanabe, Y. Takeda, H. Kobayakawa, and Y. Takashima
Department of Materials Science and Engineering, Graduate School of Engineering, Nagoya University, Nagoya 464-8603, Japan

H. Horinaka and T. Matsuyama
Department of Physics and Electronics, Faculty of Engineering, Osaka Prefecture University, Osaka 599-8531, Japan

K. Togawa
R. Kagaku Kenkyusho (RIKEN)/SPring-8, Harima Institute, Hyogo 679-5148, Japan

T. Saka
Daido Institute of Technology, Nagoya 457-8531, Japan

M. Tawada, T. Omori, Y. Kurihara, and M. Yoshioka
High Energy Accelerator Research Organization (KEK), Tsukuba 305-0801, Japan

K. Kato
Daido Steel Co. Ltd., Nagoya 457-8531, Japan

T. Baba
Silicon Systems Research Laboratories, NEC Corporation, 1120, Simokuzawa, Sagamihara, Kanagawa 220-1198, Japan

(Received 10 November 2004; accepted 14 February 2005; published online 20 April 2005)

GaAs–GaAsP and InGaAs–AlGaAs strained-layer superlattice photocathodes are presented as emission sources for highly polarized electron beams. The GaAs–GaAsP cathode achieved a maximum polarization of 92(±6)% with a quantum efficiency of 0.5%, while the InGaAs–AlGaAs cathode provides a higher quantum efficiency (0.7%) but a lower polarization [77(±5)%]. Criteria for achieving high polarization using superlattice photocathodes are discussed based on experimental spin-resolved quantum efficiency spectra. © *2005 American Institute of Physics*. [DOI: 10.1063/1.1886888]

I. INTRODUCTION

At present, polarized electron beams are conventionally produced by photoemission from GaAs-type semiconductors. This type of polarized electron source (PES) is based on a combination of two fundamental technologies; optical pumping by circular laser photons, and emission of conduction electrons into vacuum using a special surface with negative electron affinity (NEA). Bulk GaAs is a direct-gap semiconductor with degenerate heavy-hole (hh) and light-hole (lh) bands at the valence-band maximum (Γ point) and maximum electron-spin polarization (ESP) is limited to be 50%. This degeneracy can be resolved through the use of a strained GaAs layer, an unstrained superlattice structure, or a strained superlattice structure, for which our group previously achieved experimental ESPs of 86%,[1] 70%,[2] and 83%,[3] respectively.

In our studies it became clear that by using a modulation-doping method, the GaAs–AlGaAs superlattice (SL) cathode is capable of achieving much higher quantum efficiency (QE) than the strained GaAs layer. Thus, while heavy doping is used for surface layers to achieve large band bending, medium doping is better for SL layers in order to avoid spin-flip depolarization. More importantly, however, SL cathodes were found to provide a solution for the surface charge limit (SCL) problem, whereby the maximum current density that can be extracted from the NEA surface is much lower than that determined by the space-charge effect.[4] This effect is caused by a decrease in band bending at the NEA surface due to the surface photovoltage (SPV) effect. However, a GaAs$-$Al$_{0.35}$Ga$_{0.65}$As (SL 7) cathode has been demonstrated to produce a space-charge-limited current of 14 A (2.3×10^{11} e in a 2.5-ns bunch) using a 120-keV gun with a QE of 2.0% at a laser wavelength of 752 nm.[5] This means that the use of a modulation-doped SL photocathode solves the SCL problem for this beam condition.

Encouraged by these results, the present authors have continued research on the development of types of InGaAs–AlGaAs (Ref. 6) and GaAs–GaAsP-strained SL structures. We have also investigated the SCL problem in more detail using GaAs–AlGaAs and InGaAs–AlGaAs SL photocath-

[a]FAX: +81-52-789-2897; electronic mail: nakanisi@spin.phy.nagoya-u.ac.jp

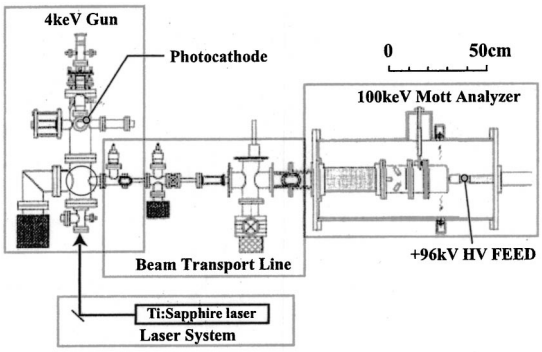

FIG. 1. A schematic view of a cathode test system at Nagoya University.

odes irradiated by a nanosecond double-bunch laser with 2.8-ns separation time.[7,8] In this paper, we describe experimental results demonstrating the improvements in ESP, QE, and SCL effect achieved using a GaAs–GaAsP cathode. Criteria for obtaining the highest ESP are also proposed based on spin-resolved QE spectra obtained experimentally for GaAs–AlGaAs, InGaAs–AlGaAs, and GaAs–GaAsP SL photocathodes.

II. EXPERIMENTAL PROCEDURES

ESP and QE spectra were measured using a compact cathode test system as shown in Fig. 1. The system consists of a diode-laser-pumped Ti:sapphire continuous-wave (cw) laser, a 4-keV gun, a beam transport line with a spin rotator, and a standard 100-keV Mott polarimeter.[9] The base pressure was set at $\sim 2\times 10^{-10}$ Torr after baking the gun chamber at 200 °C for 30 h.

The InGaAs–AlGaAs SL samples were fabricated by molecular-beam epitaxy (MBE) at NEC, and the GaAs–GaAsP SL samples were made by metal-oxide chemical-vapor deposition (MOCVD) at laboratories of Nagoya University and Daido-Steel Company. The InGaAs–AlGaAs sample was prepared with a protective surface film of amorphous As, which was removed by heat cleaning at 400 °C in a vacuum. The GaAs–GaAsP sample had no protective film and was heat cleaned at 550 °C for 2 h in a vacuum. Small amounts of cesium and oxygen were supplied to obtain NEA surfaces by the "Yo-Yo" method. The QE was monitored by simultaneous measurement of photocurrent and irradiation laser power, and the ESP was measured using a 100-keV Mott analyzer with 6 Au-foil targets for self-calibration of the effective Sherman function. The maximum systematic error for this ESP measurement was estimated to be ±6% (absolute value).

A number of different SL samples with various materials and crystal parameters were fabricated and tested, from which two samples from each of the InGaAs–AlGaAs and GaAs–GaAsP groups were selected for detailed analysis: SLSA 2 and SLSA 3 from the former group, and SLSP 9 and SLSP 16 from the latter group.

The design parameters for each sample are given in Table I. The parameters included component ratios for In, Ga, Al, As, and P elements in the surface and SL layers, thicknesses of the well and barrier layers (L_w and L_b), surface layer thickness (L_s), densities (n) of p-type doping in the surface and SL layers, and pair numbers (N_p) for the SL layers. The modulation doping technique was employed for whole samples. Be was employed for the SLSA samples and Zn for the SLSP samples as p-type dopant. The thicknesses of the wells and barrier layers were chosen so as to obtain large hh–lh energy splitting, and the total thickness of the samples was approximately 100 nm, set to minimize spin depolarization. The thicknesses of the wells and barrier layers and the component ratios of elements were checked after sample fabrication and confirmed by standard x-ray analysis.

The crystal structure and doping densities for SLSP 9 are shown schematically in Fig. 2. A commercially available GaAs wafer with high Zn dopant content was used as a substrate, and a strain-relaxed GaAsP buffer layer was formed on it to obtain large strains for the GaAs well layers. The 16 pairs of SL layers with medium Zn doping of $1.5\times 10^{18}/\mathrm{cm}^3$ were terminated with a heavily doped surface layer of GaAs (Zn $6.0\times 10^{19}/\mathrm{cm}^3$) to obtain a large band bending at the NEA surface.

TABLE I. List of specifications for InGaAs–AlGaAs and GaAs–GaAsP samples.

	SLSA 2		SLSA 3	
Surface	$In_{0.15}Ga_{0.85}As$, $L_s=4.8$ nm, $n(Be)=3.8\times 10^{19}$ cm^{-3}			
	Well layer	Barrier layer	Well layer	Barrier layer
SL layer	$In_{0.15}Ga_{0.85}As$	$Al_{0.38}Ga_{0.62}As$	$In_{0.15}Ga_{0.85}As$	$Al_{0.36}Ga_{0.64}As$
	$L_w=1.4$ nm	$L_b=3.1$ nm	$L_w=2.0$ nm	$L_b=3.1$ nm
	$n(Be)=6.0\times 10^{17}$ cm^{-3}	$n(Be)=5.8\times 10^{17}$ cm^{-3}	$n(Be)=4.6\times 10^{17}$ cm^{-3}	$n(Be)=4.5\times 10^{17}$ cm^{-3}
	$N_p=20$		$N_p=18$	
	SLSP 9		SLSP 16	
Surface	GaAs, $L_s=5$ nm, $n(Zn)=6.0\times 10^{19}$ cm^{-3}			
	Well layer	Barrier layer	Well layer	Barrier layer
SL layer	GaAs	$GaAs_{0.68}P_{0.34}$	GaAs	$GaAs_{0.67}P_{0.33}$
	$L_w=3.2$ nm	$L_b=3.2$ nm	$L_w=3.8$ nm	$L_b=3.8$ nm
	$n(Zn)=1.5\times 10^{18}$ cm^{-3}		$n(Zn)=1.5\times 10^{18}$ cm^{-3}	
	$N_p=16$		$N_p=12$	

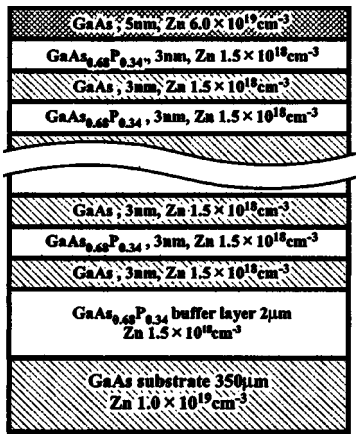

FIG. 2. Crystal structure and doping densities of the SLSP 9 sample.

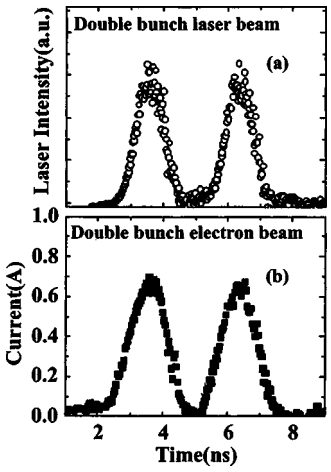

FIG. 4. Profiles of double bunch beam of laser and electron produced by using the GaAs–GaAsP cathode.

III. EXPERIMENTAL RESULTS

The ESP and QE spectra for the SLSP and SLSA cathodes are shown in Fig. 3 against the laser wavelength. The general trend is for the QE to rise at a laser wavelength corresponding to the band-gap energy, and for the ESP to peak at the QE threshold. Both of the SLSP cathodes achieved maximum ESPs of higher than 90%, with SLSP 16 reaching 92% with a QE of 0.5% at 778 nm. The SLSA cathodes showed lower ESPs of around 80%, but the highest QE of 0.7% was reached by SLSA 2 at 741 nm with an ESP of 77%.

The reduction of the SCL effect is indispensable for realizing polarized electron beams with sufficient current density for future electron-positron linear colliders, which will require intense multibunch beams with separation times of 1.4 or 2.8 ns.[10] Systematic research on the reduction of the SCL effect through the use of GaAs–AlGaAs and InGaAs–AlGaAs cathodes has already been reported by the present authors.[7,8] Here, we demonstrated that such a multibunch beam could be also produced using GaAs–GaAsP photocathodes in combination with a 50-keV gun and a 0.7-ns double-bunch laser, as shown in Fig. 4.

The full surface of a 14-mm-diameter photocathode was irradiated with a double-bunch laser at energy of 2.6 μJ/bunch and a wavelength of 773 nm. The full width at half maximum of the laser bunch was set at 0.7 ns with separation of 2.8 ns between double bunches in order to satisfy the prospective requirements of linear colliders. The electron double bunches were all of the same pulse height and symmetrical shape. The peak current of $\sim$0.7 A ($\sim$8.6 $\times 10^9$ e/bunch) and bunch width of $\sim$1.2 ns were determined by the space-charge effect of the 50-keV gun. Thus, the degradation of band bending due to the SPV effect is negligible for this cathode.

Recently, this SPV effect for SLSP 16 was studied by another approach using core-level photoelectron spectroscopy in combination with synchrotron radiation and a laser.

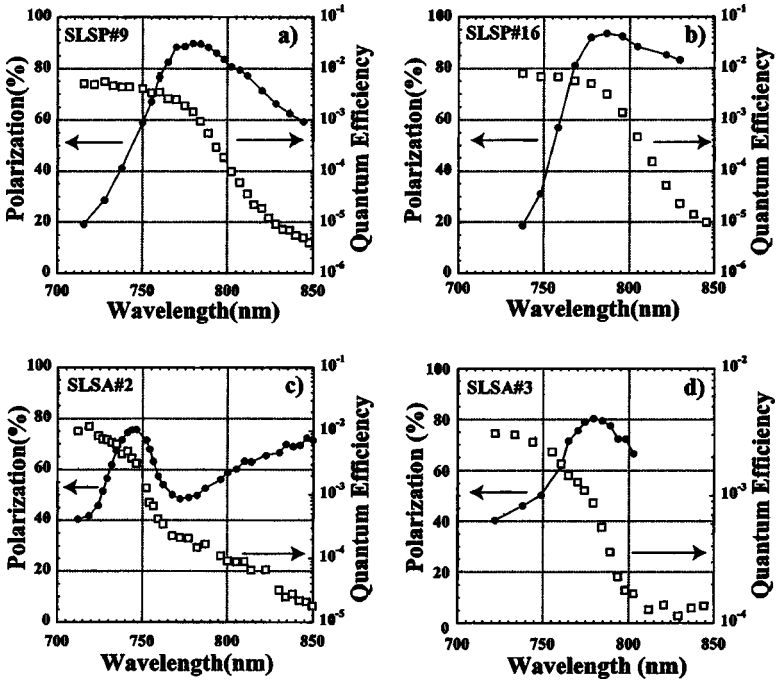

FIG. 3. Observed ESP and QE spectra, (a) and (b) for SLSP 9 and 16, and (c) and (d) for SLSA 2 and 3, respectively. The data points of ESP and QE spectra are indicated by closed circles (●) and open squares (□), respectively.

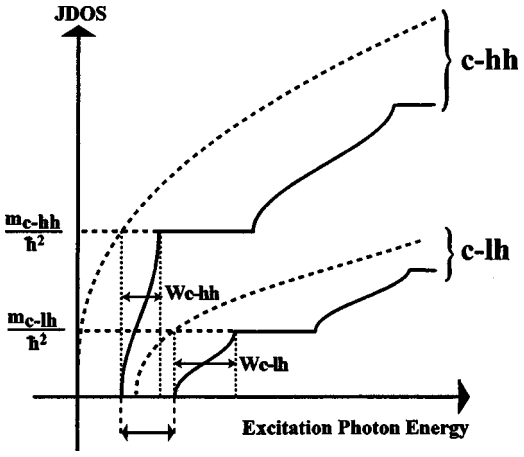

FIG. 5. Schematic behaviors of JDOSs as functions of excitation photon energy for strained layer (dotted line) and strained SL layer (solid line) in threshold energy region. Both widths of absorption edge are also indicated for the hh and lh absorption.

It was found that for liquid-nitrogen temperature the SPV effect in the SL cathode is remarkably suppressed compared with that in a bulk-GaAs cathode with Zn dopants of 1×10^{19}.[11]

IV. DATA ANALYSIS

We have experimentally investigated SL photocathodes with GaAs–AlGaAs, InGaAs–AlGaAs, and GaAs–GaAsP structures, and the highest ESPs obtained by these samples are 70%, 83%, and 92%, respectively. The maximum ESP does not equal but depends strongly on the initial polarization (P_i) of excited electrons in the conduction band, and P_i is in turn related to the coefficients of photoabsorption from the hh ($A_{\rm hh}$) and lh ($A_{\rm lh}$) minibands. The explicit relations are given by $A_{\rm hh}=A_i(1+P_i)/2$ and $A_{\rm lh}=A_i(1-P_i)/2$, where A_i is the total absorption coefficient, and the sign of P_i is defined as positive for left-handed electrons.

These photoabsorption coefficients $A_{\rm hh}$ and $A_{\rm lh}$ are proportional to the joint densities of state (JDOS) between conduction and hh or lh bands.[12] The typical behaviors of these JDOSs in the threshold region are shown in Fig. 5, where the two dotted lines represent the JDOSs for strained layers, and the two solid lines denote those for strained SL layers. The latter exhibit a series of quantum jumps with a unit of $m/(\pi\hbar^2)$, where m is a reduced mass defined as $m_{c\text{-hh}}=(m_c\times m_{\rm hh})/(m_c+m_{\rm hh})$ for hh absorption, and $m_{c\text{-lh}}=(m_c\times m_{\rm lh})/(m_c+m_{\rm lh})$ for lh absorption. The width of the absorption edge ($W_{c\text{-hh}}$ or $W_{c\text{-lh}}$) corresponds to the sum of widths for both the conduction and the hh or lh minibands.

For comparison of the experimental data with the above JDOS-based $A_{\rm hh}$ and $A_{\rm lh}$ spectra it is convenient to use the spin-resolved quantum efficiencies for left-handed (Q_L) and right-handed (Q_R) electrons in an emitted beam as functions of excitation photon energy. The Q_L and Q_R spectra are related to the experimental ESP and QE spectra by $Q_L=\mathrm{QE}(1+\mathrm{ESP})/2$ and $Q_R=\mathrm{QE}(1-\mathrm{ESP})/2$, where the sign of ESP is defined as positive for left-handed electrons. If the depolarization effect inside the cathode crystal is small, we can expect that the Q_L and Q_R spectra will exhibit quite similar behavior to the corresponding JDOS spectra. For the analysis of polarized photoluminescence, a similar method was employed earlier.[13]

The experimental Q_L and Q_R spectra are plotted in Fig. 6. As expected from the typical JDOS spectra in Fig. 5, a steplike jump in QE is clearly observed in the Q_L spectra for both the SLSP cathodes, yet is difficult to discern for the SLSA cathodes. No such QE steps were observed in any of the Q_R spectra, probably due to the limited range of wavelengths covered by our laser system.

The parameters of the JDOS-based $A_{\rm hh}$ and $A_{\rm lh}$ spectra were determined for the SLSP cathodes using threshold energies for hh and lh excitations calculated by the Kronig–Penny (KP) model,[14] by approximating the shapes and widths of the hh and lh absorption edges by dispersion-relation curves calculated using the KP model, and by modeling the unit of quantum absorption jump as being proportional to $m/(\pi\hbar^2)$ after the observed jump in QE. Table II lists the parameters calculated using the KP model: threshold energy ($E_{\rm th}$) and corresponding laser wavelength (λ), hh–lh energy splitting (δ), and widths W_c, $W_{\rm hh}$ and $W_{\rm lh}$ for the conduction, hh and lh minibands, respectively.

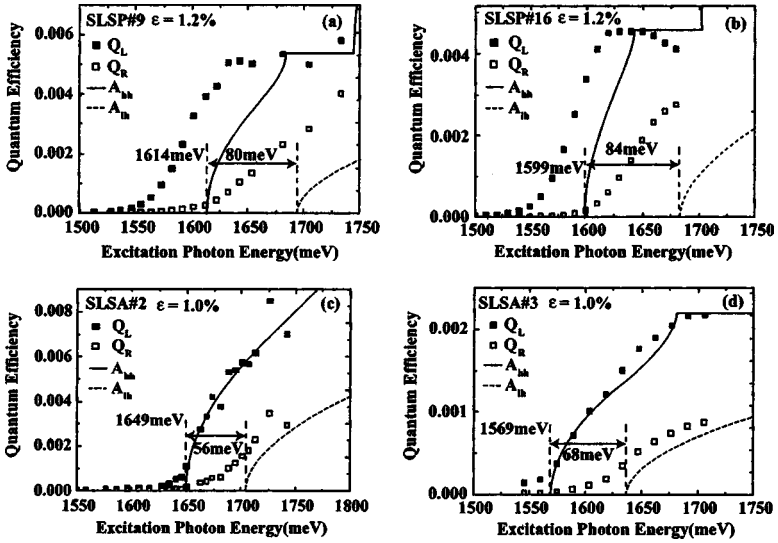

FIG. 6. The $Q_{\rm L}$ and $Q_{\rm R}$ spectra (experimental) and the JDOS-based $A_{\rm hh}$ and $A_{\rm lh}$ spectra (calculated), where (a) and (b) for SLSP and (c) and (d) for SLSA cathodes.

TABLE II. Mini-band parameters calculated by the Kronig–Penny model for each sample.

	SLSP 9	SLSP 16	SLSA 2	SLSA 3
Eth (eV)	1.61	1.60	1.57	1.54
λ(nm)	770	770	790	805
δ(meV)	81	84	67	37
W_{hh}(meV)	3.5	0.5	9.1	4.8
W_{lh}(meV)	80	35	113	85
W_c(meV)	81	35	107	74

The calculated JDOS-based A_{hh} and A_{lh} spectra for the SLSP cathodes are shown in Fig. 6. The threshold positions for the Q_L and Q_R spectra do not coincide with those of the A_{hh} and A_{lh} spectra, instead being shifted to lower photon energies. This discrepancy can be resolved by taking the strain relaxation effect into account. The critical thickness with respect to strain relaxation can be estimated using the Matthews and Blakeslee's formula.[15] A net strain (ε^*) is defined for the SL layer as $\varepsilon^* = \varepsilon L_w/(L_w + L_b)$, where L_w and L_b are the widths of the well and barrier layers, respectively, and ε is the strain induced by lattice mismatch between the well and barrier layers. The estimated values of strain, net strain, and critical thickness for each sample are listed in Table III, together with the total thickness of the SL layers.

The SLSA sample has a critical thickness about three times that for the SLSP cathodes. The total thickness of the SLSP sample is about five times larger than the critical thickness, and significant strain relaxation is expected to occur in the sample. In fact, a number of small cracks on the surface were observed for these samples. As shown in Fig. 7, reasonable agreement is obtained for the threshold positions if the reduced strains after relaxation are assumed to be 0.66% and 0.72% for SLSP 9 and SLSP 16, respectively. This degree of strain relaxation is reasonable considering that appreciable relaxation has already been observed for a strained GaAs layer on a GaAsP buffer layer.[16]

As can be seen in Fig. 6, no steplike QE jump was observed in the Q_L spectra for the SLSA cathodes. Therefore, the A_{hh} spectra can be expected to fit to the Q_L spectra by treating the unit of quantum absorption jump as a free parameter. The fitted absorption spectra are shown in Fig. 6. In contrast to the SLSP cathodes, the Q_L threshold energy agrees quite well with that calculated by the KP model. The total thickness is less than twice the critical thickness for the SLSA samples, and strain relaxation seems to be less important.

The Q_R spectra for the SLSA cathodes in Fig. 6 and the SLSP cathodes in Fig. 7 (after adjustment) show that the threshold position is smeared by small amounts of right-handed electrons below the threshold energy level. These right-handed electrons appear to be created from left-handed electrons through spin-flip interactions, and this smearing effect looks to be an important factor determining the upper limit of ESP.

TABLE III. Estimated values of strain, net strain, and critical thickness for each SL sample.

	SLSP 9	SLSP 16	SLSA 2	SLSA 3
Strain (ε)	1.2	1.2	1.0	1.0
Net strain (ε^*)	0.60	0.60	0.22	0.25
Critical thickness (nm)	20	20	66	57
Total thickness (nm)	107	98.6	98.7	99.9

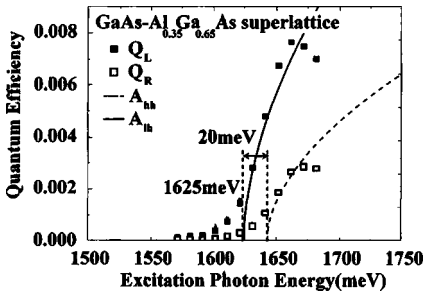

FIG. 8. The Q_L and Q_R spectra obtained by the SL 7 cathode.

The relatively low ESP (~70%) for the GaAs–$Al_{0.35}Ga_{0.65}As$ (SL 7) cathode can be understood from the Q_L and Q_R spectra (Fig. 8).

As SL 7 is a nonstrained-layer SL sample, the calculated hh–lh energy splitting ($\delta \sim 20$ meV) is much smaller than for the SLSA and SLSP samples. As a result, the overlap between the Q_L and Q_R spectra in the threshold region becomes more prominent, and it is thought that this overlapping effect limits the ESP of nonstrained-layer SL cathodes.

From the above data analyses, it was clarified that the experimental Q_L and Q_R spectra for three types of SL photocathodes (GaAs–GaAsP, InGaAs–AlGaAs, and GaAs–AlGaAs) could be well fitted by the calculated photoabsorption A_{hh} and A_{lh} spectra in the excitation photon energy region of this experiment. The steplike QE jump predicted in the A_{hh} spectrum was clearly observed in the experimental Q_L spectra for both the GaAs–GaAsP photocathodes.[17]

The mechanism that determines the maximum ESP is also understood clearly by the help of data analyses of spin-resolved QE spectra. Comparing the experimental Q_L and Q_R spectra for three types of SL photocathodes with different maximum polarizations, it was confirmed that the most important factors for achieving high ESP are (1) large hh–lh separation energy (δ), (2) narrow joint widths (denoted as $W_{c\text{-hh}}$ in Fig. 5) between the conduction and hh minibands, and (3) minimal depolarization interactions inside the SL layers. Combining factors (1) and (2), a condition of $\delta \geqslant W_{c\text{-hh}}$ was derived as the single most important condition to achieve high ESP and high QE, that is, suppressing the overlap between the A_{hh} and A_{lh} absorptions. Condition (3) is

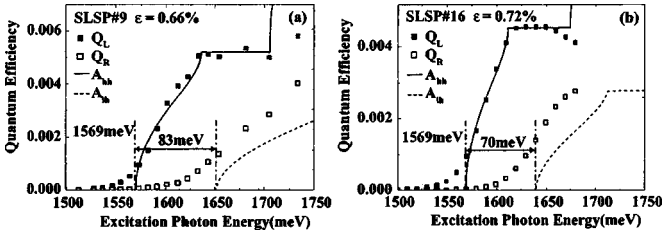

FIG. 7. The Q_L and Q_R spectra with the shifted threshold energies calculated by using the reduced strains for SLSP samples.

required to reduce the smearing effect in the Q_R threshold region. The above criteria explain why the GaAs–GaAsP-strained SL photocathode can achieve such high ESP and QE simultaneously.

V. SUMMARY

This paper continues our systematic study of strained-layer SL photocathodes with InGaAs–AlGaAs and GaAs–GaAsP structures. The highest ESP of 92% was obtained using a GaAs–GaAsP cathode, with a QE of 0.5% at a laser wavelength of 778 nm. A slightly higher QE of 0.7% was obtained using an InGaAs–AlGaAs sample at 741 nm, although with a lower ESP of 77%. Both cathodes exhibited strong resistance to the SCL effect and were capable of producing nanosecond double-bunch beams of polarized electrons with a peak current of ~1 A. These results confirm that GaAs–GaAsP SL photocathodes are capable of delivering electron beams with high ESP, high QE, and high peak current, suitable for injection into high-energy accelerators. This cathode is particularly promising for application to future electron-positron linear colliders.

The phenomenological data analyses of spin-resolved QE spectra help to understand the mechanism which determines the ESP and QE. Comparing the experimental Q_L and Q_R spectra with the calculated photoabsorption A_{hh} and A_{lh} spectra, it was confirmed that the most important factors for achieving high ESP are (1) large hh–lh separation energy (δ), (2) narrow joint widths between the conduction and hh minibands, and (3) minimal depolarization interactions inside the SL layers.

Further experiments involving measurement of the dependence of the maximum ESP and QE attained by the GaAs–GaAsP cathodes on the SL layer thickness are currently in progress, and the detailed evaluation of crystal quality and its influence on PES performances are also continuing. The results of these studies will be published in forthcoming papers. Further development of the data analysis procedure is also required in order to clarify the physical mechanisms that dominate PES performances in terms of ESP, QE, and resistance to SCL effects for strained-layer SL cathodes.[18] The source emittance and lifetime of NEA–GaAs photocathodes are also subjects of attention, as improvements of these features are required urgently for future applications such as the Energy Recovery Linac-based light source project.

ACKNOWLEDGMENTS

The authors extend their gratitude to Dr. R. Oga, T. Gotoh, and M. Katsuki of Nagoya University for valuable support during this experiment. We thank Dr. M. Kamada of Saga University for collaboration in an experiment examining the SPV effect, and thank Professor H. Sugawara, Professor Y. Kimura, Professor Y. Kamiya, and Professor S. Kurokawa of KEK and Professor I. Sanda of Nagoya University for continuous encouragement as part of the GLC-R/D project. This work was supported by Grants-in-Aid for Scientific Research (Grant Nos. 10354003 and 15204019) from the Ministry of Education, Culture, Sports, Science, and Technology of Japan and a series of research funds from KEK for the cooperative development of polarized electron sources (1998-2003).

[1] T. Nakanishi, H. Aoyagi, H. Horinaka, Y. Kamiya, T. Kato, S. Nakamura, T. Saka, and M. Tsubata, Phys. Lett. A **158**, 345 (1991).
[2] T. Omori *et al.*, Phys. Rev. Lett. **67**, 3294 (1991).
[3] T. Omori *et al.*, Jpn. J. Appl. Phys., Part 1 **33**, 5676 (1994).
[4] M. Woods *et al.*, J. Appl. Phys. **73**, 8631 (1993).
[5] Y. Kurihara *et al.*, Jpn. J. Appl. Phys., Part 1 **34**, 355 (1995).
[6] T. Nakanishi *et al.*, AIP Conf. Proc. **421**, 300 (1998).
[7] K. Togawa *et al.*, Nucl. Instrum. Methods Phys. Res. A **414**, 431 (1998).
[8] K. Togawa *et al.*, Nucl. Instrum. Methods Phys. Res. A **455**, 118 (2000).
[9] T. Nakanishi *et al.*, Jpn. J. Appl. Phys., Part 1 **25**, 766 (1986).
[10] GLC group, GLC Project Report, 139 (2003), JLC group KEK-Report 97-1 (1997).
[11] S. Tanaka, T. Nishitani, T. Nakanishi, S. D. More, J. Azuma, K. Takahashi, O. Watanabe, and M. Kamada, J. Appl. Phys. **95**, 551 (2004).
[12] M. A. Fox, *Optical Properties of Solids*, Oxford Master Series in Physics (Oxford University Press, Oxford, 2001), p. 53.
[13] R. A. Mair, R. Prepost, E. L. Garwin, T. Maruyama, Phys. Lett. A **239**, 277 (1998); T. Matsuyama, H. Horinaka, K. Wada, T. Kondo, M. Hangyo, T. Nakanishi, S. Okumi, K. Togawa, Jpn. J. Appl. Phys., Part 2 **40**, L555 (2001).
[14] G. Bastard, Phys. Rev. B **24** 5693 (1981).
[15] J. W. Matthews and A. E. Blakeslee, J. Cryst. Growth **27**, 118 (1974); M. Ogasawara, H. Sugiura, M. Mitsuhara, M. Yamamoto, and M. Nakao, J. Appl. Phys. **84**, 4775 (1998).
[16] H. Aoyagi *et al.*, Phys. Lett. A **167**, 415 (1992).
[17] T. Nakanishi *et al.*, Proceedings of LINAC 2004, Luebeck, 16–20 August 2004 (unpublished), THP24.
[18] A. D. Andreev and A. V. Subashiev, Physica E (Amsterdam) **13**, 556 (2002).